Density Functional Theory Study of Epitaxially Strained Monolayer Transition Metal Chalcogenides for Piezoelectricity Generation

Yanfu Lu[1,3], *Susan B. Sinnott*[1,2,3*]

1. Department of Materials Science and Engineering, The Pennsylvania State University, University Park, PA 16802 USA
2. Department of Chemistry, The Pennsylvania State University, University Park, PA, 16802, USA
3. Materials Research Institute, The Pennsylvania State University, University Park, PA, 16802, USA

* Address correspondence to sbs5563@psu.edu

KEYWORDS Epitaxial strain, transition metal chalcogenides, piezoelectricity, density functional theory, 2D materials.

ABSTRACT

Two-dimensional transition metal chalcogenides (2D TMCs) are known for their wide range of bandgaps, flexibility, and high strength. Recent synthesis and data mining efforts indicate that 56 2D TMCs have low exfoliation energies and are relatively stable in monolayer form. Under epitaxial strain, we predict using density functional theory (DFT) calculations that the majority of these 2D TMCs can accommodate ±10% strain without breaking their crystal symmetry. The elastic and piezoelectric tensors indicate that 22 of 56 candidates are piezoelectric and we derive their in-plane piezoelectric coefficient d_{11}. The epitaxial strain is further predicted to enhance the d_{11} by over 100% at 10% tensile epitaxial strain for most of these piezoelectric 2D TMCs. $ReSe_2$ at pristine state and Au_2Se_2 at +5% epitaxial strain are predicted to obtain the extreme d_{11} coefficients at -120 pm/V and 326 pm/V, respectively. These findings have implications for the use of high-performance 2D piezoelectric materials in devices.

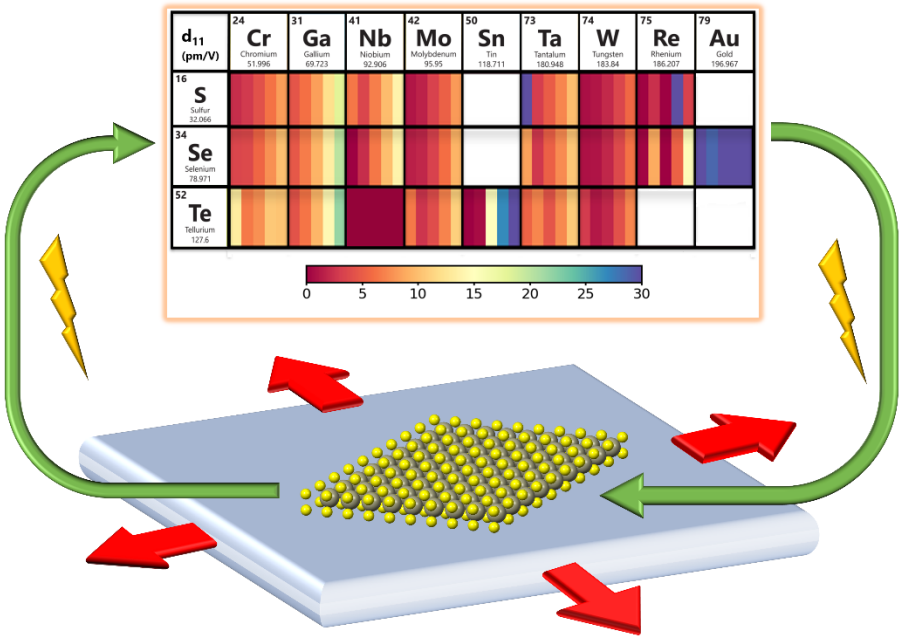

Introduction

Semiconducting transition metal chalcogenides (TMCs) exhibit unique properties in two-dimensional (2D) form relative to the bulk.[1–3] Atomically thin TMCs not only have bandgap energies that span a wide range of values from meV to several eV but also have extremely small bending rigidity and relatively high Young's modulus.[4] Several experimental studies have investigated the effect of strain on 2D TMCs[5] and explored flexible device applications,[6,7] such as wearable sensors [8,9] and electronic skin.[10] The focus has been on in-plane uniaxial strain[11,12] with few studies considering in-plane epitaxial strain.[13,14] Compared to uniaxial strain, the advantages of epitaxially strained 2D TMCs include unchanged crystal symmetry, tunable bandgaps with the same crystal momentum as the pristine state,[13] and the potential to stack the layers in a confined heterostructure.[14]

One particularly motivating strain-related property is piezoelectricity.[15,16] The prerequisites of piezoelectric materials are broken inversion symmetry and non-metallic electronic bandgap. Piezoelectric 2D TMCs show great promise in the design of 2D piezoelectric devices. For example, combining photoelectric and piezoelectric properties, monolayer MoS_2 becomes a candidate for optoelectronics[17] and piezo-phototronics.[18] The piezoelectricity of 2D materials can be further engineered by introducing surface defects and adatoms.[19,20] At the same time, defects can dramatically alter other properties, such as bandgap and Young's modulus, and cannot be easily controlled.[21]

In recent years, over 32 new TMCs have been synthesized and these are cataloged in a library of atomically thin TMCs.[22] High-throughput first-principles calculations play an important role in screening for possible 2D materials based on exfoliation energy and the number of atoms in the crystal unit cell.[23] From 108,423 unique, experimentally known 3D compounds from the Inorganic Crystal Structure Database (ICSD),[24] only 56 compounds have 1) certain plane with

exfoliation energy below 200 meV/Å^2, 2) only two elements consisted of a transition metal and a chalcogenide element. The library of 2D TMCs is not necessarily limited to these 56 compounds because of the possibility of undiscovered crystal structures and unknown confined heterostructures. For example, in epitaxial growth, the substrate selection can particularly decrease the nucleation energy of a metastable phase with dramatically different physical or chemical properties compared to the ground state.[25]

Here, we investigate epitaxial strain engineering and enhanced piezoelectricity of 2D monolayer TMCs using density functional theory (DFT) calculations.[26] In particular, the crystal structure and formation energy at both ground state and epitaxially strained states are examined as references for heterostructure fabrication and strain engineering. Furthermore, from the possible piezoelectric 2D TMC candidates, the potential piezoelectric enhancement from epitaxial strains is determined. The results suggest that epitaxial strain may be a way to control the piezoelectricity in 2D monolayer TMCs and thus both boost the capabilities of current 2D piezoelectric devices and enable their integration into more complex MEMS devices.

Results and Discussion

The successfully synthesized and computationally predicted 56 monolayer TMCs [22,23] indicate that the symmetry of 2D monolayer TMCs follows the group number of the transition metal elements, which starts with Ti located at period 4 and group 4 in the periodic table. All the group 4 elements tend to form 2D TMCs in $P\bar{3}m1$ space group (1T structure) as the most stable structures, shown in Figure 1 (A). As the group number increases, the 2D compounds gradually transform to the $P\bar{6}m2$ space group (2H structure), illustrated in Figure 1 (B), as the most stable structures until group 7. The 2D compounds in group 5 and 6 are predicted to be transition states which both symmetries can co-exist as the stable crystal structures. After group 7, no general trend

is discovered while four other symmetries are identified including $P4/nmm$, $P2_1/c$, Pm, and $Pmn2_1$, demonstrated in Figure 1 (C)-(F). However, the majority of the stable 2D compounds favor 3-fold or 6-fold symmetry as free-standing structures.

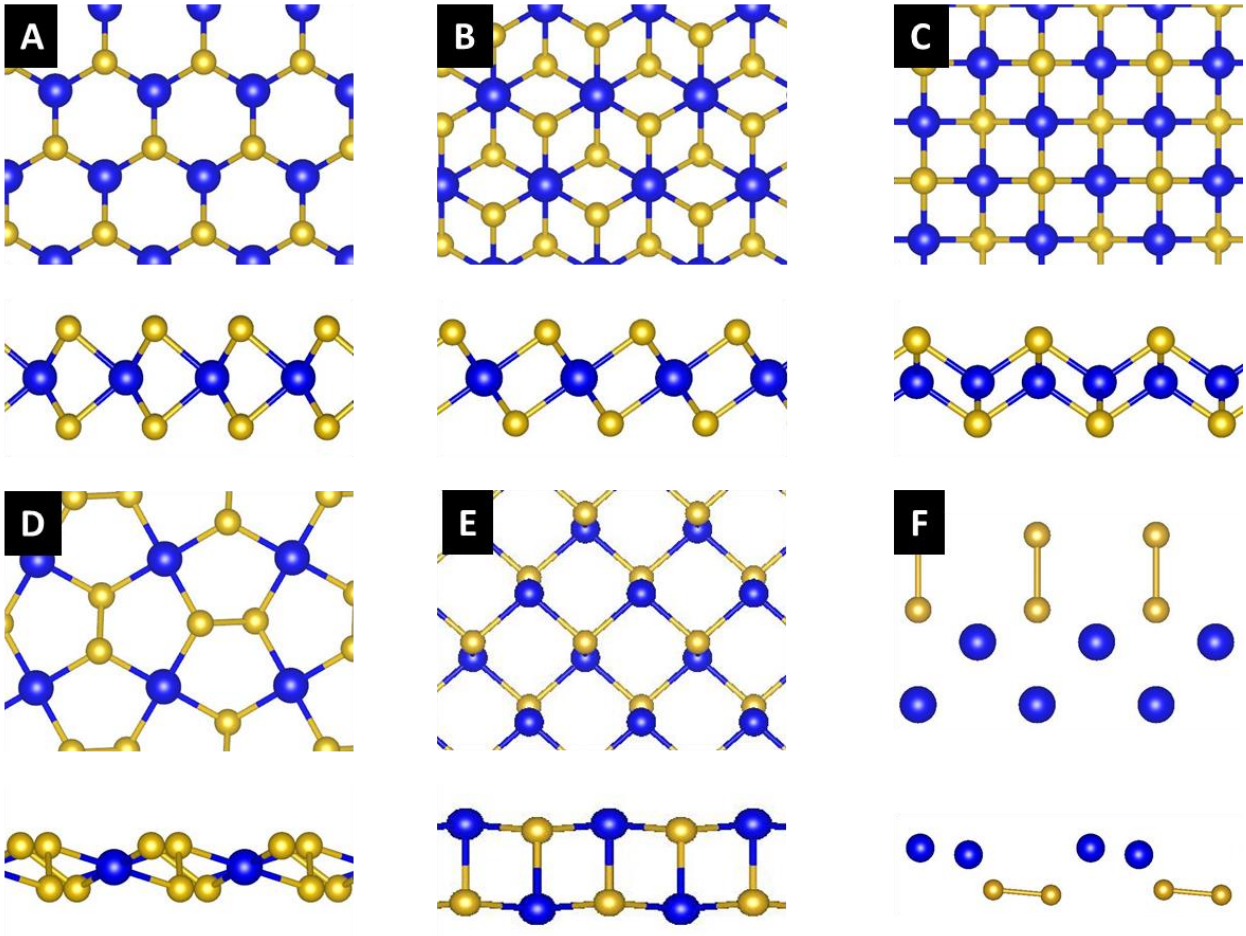

Figure 1. The top and side view of 2D transition metal chalcogenides. (A)-(F) are the crystal structures of $P\bar{3}m1$ (1T), $P\bar{6}m2$ (2H), $P4/nmm$, $P2_1/c$, $Pmn2_1$, Pm, respectively.

In Figure 2, the lattice parameters of the calculated 56 2D monolayer TMCs indicates the ways in which the atomic size of the transition metal elements and chalcogen elements influence the compound lattice parameter. Moreover, in Cr-based, Nb-based, Ta-based compounds, both $P\bar{3}m1$ and $P\bar{6}m2$ symmetry can co-exist, and the lattice parameter of $P\bar{6}m2$ symmetry is smaller

than that of $P\bar{3}m1$ symmetry in the same composition. Interestingly, except for Sn_2Te_2, all the compounds retain the same symmetry from -10% to +10% in-plane epitaxial strain. Sn_2Te_2 goes through a phase transition to $P2_1/c$, $P4/nmm$, $Pmn2_1$ space group in -10%, -9% — -2%, -1% — +10% epitaxial strain, respectively.

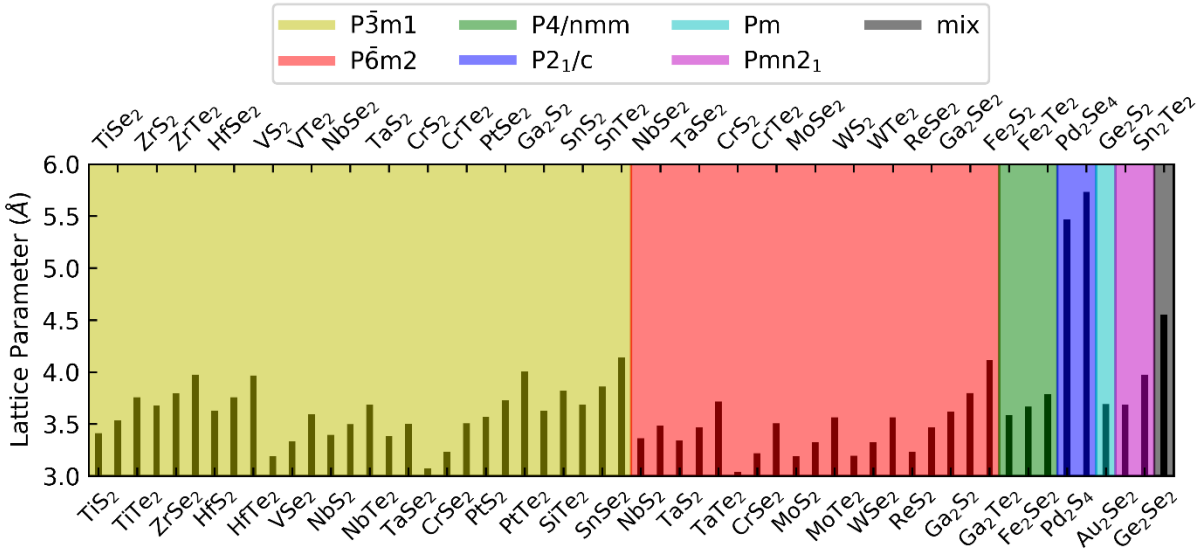

Figure 2. The lattice parameter of the calculated 56 2D monolayer transition metal chalcogenides. The colored background represents the different symmetries of the crystal structures.

In all the 56 calculated monolayer TMCs, the stability of the free-standing crystal structure is crucial for experimental synthesis. The overall stability can be discovered by the formation energy from convex hull construction, and the tendency to become free-standing monolayer can be determined from the exfoliation energy. In order to derive the formation energy of each compound, the equation, $E_f = \frac{E_{2D,M_aX_b} - a \times E_{M,bulk} - b \times E_{S_8 \, or \, Se_3 \, or \, Te_3}}{n_{atoms}}$, is applied, where E_{2D,M_aX_b} is the calculated energy of each 2D monolayer TMCs, $E_{M,bulk}$ is the calculated energy of each transition metal in the most stable bulk form, $E_{S_8 \, or \, Se_3 \, or \, Te_3}$ is the calculated energy of the most stable form of chalcogen elements, a, b are the number of atoms in the compound composition, and n_{atoms} is the total number of atoms in the system. As shown in Figure 3, for the compounds

of the same composition, the $P\bar{3}m1$ space group is more stable than the $P\bar{6}m2$ space group. The exfoliation energy represents the energy needed to peel off a monolayer from the bulk form of the material and is calculated using the following equation, $E_{exf} = \frac{E_{2D,M_aX_b} - E_{bulk,M_aX_b}}{n_{atoms}}$. Compared to formation energy, the exfoliation energy is a small fraction of formation energy in most of the calculated compounds. Meanwhile, the relatively low exfoliation energy implies free-standing monolayer on different substrates and van der Waals interactions between the layers of the compounds in the bulk form.

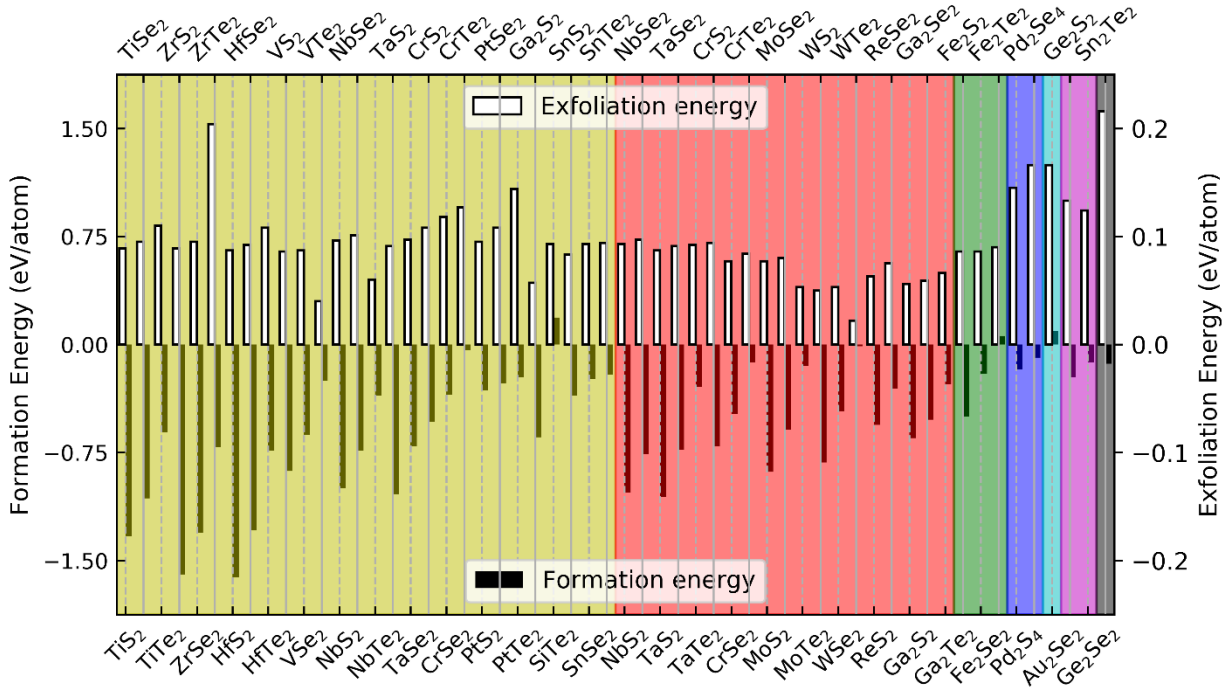

Figure 3. Exfoliation energy and formation energy of the calculated 56 2D monolayer transition metal chalcogenides. The yellow, red, green, blue, light-blue purple and gray colored background represents the $P\bar{3}m1$,$P\bar{6}m2$, $P4/nmm$, $P2_1/c$, Pm, $Pmn2_1$, and mixed symmetries of the crystal structures.

Unlike the in-plane uniaxial strained 2D TMCs, the in-plane epitaxial strain does not change the overall crystal symmetry. In order to explore the possibility of anisotropic elastic deformation, the supercell is expanded to 4×4 from the unit cell. When the epitaxial strain is

applied to the 2D monolayer TMCs, the energy difference can be obtained by the equation $E_{diff} = \frac{E_{strained} - E_{pristine}}{n_{atoms}}$. The calculated structures are the most stable phases at room temperature. No phase transformation was discovered at strained states in these ground-state calculations.

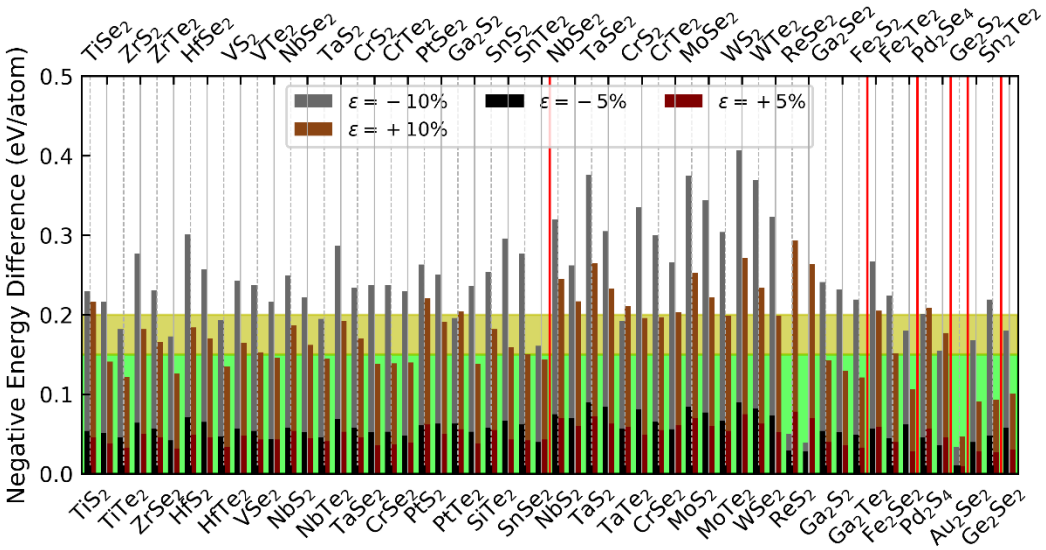

Figure 4. Energy differences at epitaxially strained states compared to the formation energy. The formation energy and strained states are represented by the white box and colored bars within the box. The red lines separate the symmetry of the crystal structure in the order of $P\bar{3}m1$,$P\bar{6}m2$, $P4/nmm$, $P2_1/c$, Pm, $Pmn2_1$, and mixed space group. The green and yellow background illustrate the energy difference of 0.15 and 0.20 eV/atom of strained states relative to the pristine state.

The energy difference is plotted inversely and directly compare with formation energy in Figure 4 to reveal the energy instability from the epitaxial strain. At ±5% epitaxial strain, all the TMC structures considered here exist in a metastable state where the inverse energy difference is smaller than the formation energy. At ±10% epitaxial strain the energy difference is a fraction of formation energy in the pristine state for the majority of the TMCs. Although very few experiments test the maximum compressive and tensile epitaxial strain that monolayer TMCs can endure, Zhang et al.[27] found that the maximum uniaxial tensile strain of WS_2 can reach 12% as derived

from the bandgap values before and after the strain was applied. To examine this case in our calculations, we elongated the WS_2 structure in either the zig-zag or arm-chair direction and determined that the energy difference between the strained and pristine states at 0.151 eV/atom and 0.175 eV/atom, respectively. By utilizing this energetic reference, it is proposed that 0.15 eV/atom is the threshold for metastable free-standing epitaxially strained monolayer TMCs. Above 0.20 eV/atom, the epitaxial strain of monolayer TMCs may result in a plastic deformation and/or defect development. These thresholds of 0.15 eV/atom and 0.20 eV/atom are highlighted in green and yellow regions, respectively, in Figure 4.

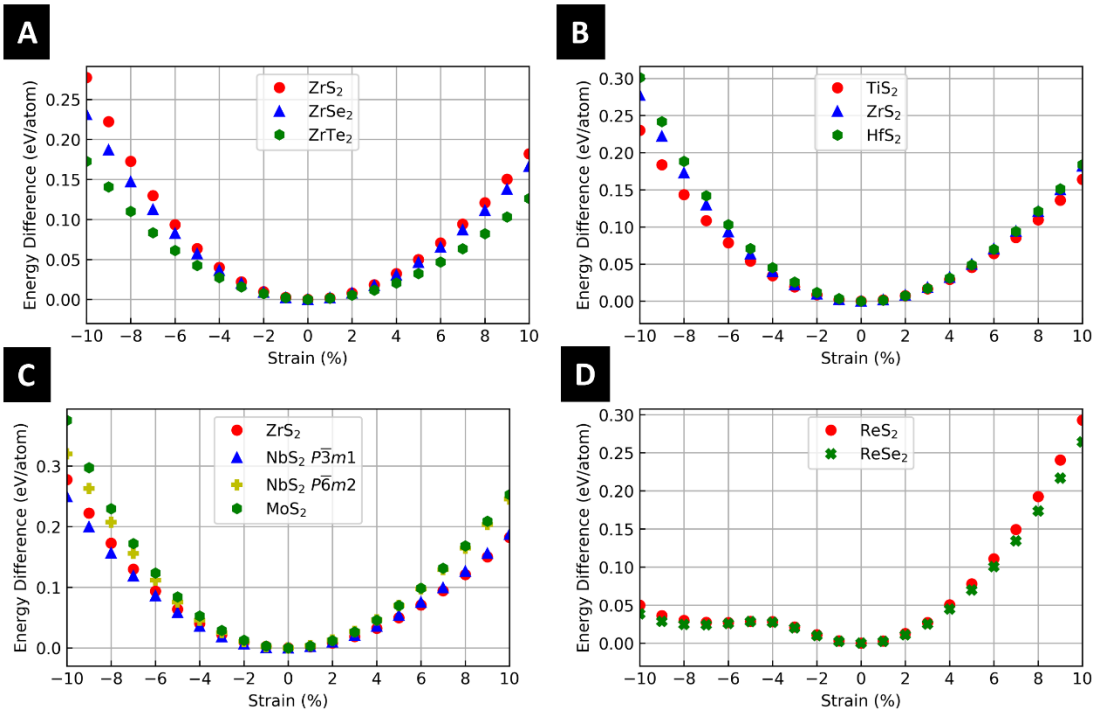

Figure 5. Energy differences from -10% to 10% epitaxial strain of the TMCs with (A) different chalcogen elements, (B) different transition metal elements in the same group, and (C) different transition metal elements in the same period. In (D), it is illustrated that the abnormal energetic behavior in Re-based chalcogenides happens in the compressive epitaxial strain region.

To explore more trends in epitaxial strained TMCs based on the periodic table, the energy difference from -10% to 10% epitaxial strain is plotted in Figure 5. The shape of the curves is

parabolic due to the interatomic potential. The repulsion between atoms is stronger than the attraction. Thus, the compressive strain is more energy sensitive than the tensile strain. In Figure 5A, by analyzing different chalcogen elements in TMCs, the larger chalcogen atom results in less energy difference at all epitaxial strain when transition metal elements remain the same. However, the larger transition metal atom in the same group results in more energy difference at all epitaxial strain when the chalcogen element remains the same, presented in Figure 5B. When the transition metal elements in the same period are investigated in Figure 5C, the similar trend in atom size of transition metal elements is discovered. Moreover, the hexagonal crystal structure is more energetically sensitive than the trigonal crystal structure at all epitaxial strain when the composition remains the same. Of all the monolayer TMCs, only Re-based chalcogenides demonstrate an abnormal energetic behavior in the compressive epitaxial strain region. Not only the trend of chalcogen atom size is reversed, but also an energetic plateau appears at -7% epitaxial strain. This local energy minimum state is only 0.03 eV/atom above the ground state. The crystal structure of the local energy minimum state is interestingly the same as that of ground state while the monolayer thickness is increased by 0.395 Å. All the other monolayer TMCs change the thickness within 0.1 Å across all the epitaxial strain. Different from black phosphorus, the crystal structural change of Re-based chalcogenides is isotropic instead of anisotropic. Therefore, instead of a structural phase transformation, a new metastable phase of Re-based chalcogenides is predicted at compressively strained state.

An important property related to mechanical strain is piezoelectricity. Some of the calculated TMCs belong to a centrosymmetric point group and thus cannot be piezoelectric. Only point groups of m and 3m are non-centrosymmetric, and the related piezoelectric coefficients, e_{ij} (pC/m) and d_{ij} (pm/V) in Voigt notation, can be nonzero. The relaxed ion elastic and piezoelectric

stress tensors, C_{ij} and e_{ij}, are acquired from the sum of ionic and electronic contributions. If the in-plane directions x_1 and x_2 are defined as the armchair and zigzag direction in the $\bar{6}m2$ symmetry, the piezoelectric strain tensor is derived to only one nonzero coefficient, $d_{11} = -d_{12} = -d_{26} = e_{11}/(C_{11} - C_{12})$, based on the point group symmetry and intrinsic 2D monolayer structure.[28] Similarly, the m point group in the primitive unit cell, the piezoelectric coefficients are reduced to d_{11}, d_{12}, d_{13} and d_{15} in the 2D monolayer structure. However, only d_{11} is the dominant coefficient compared to other coefficients. The same results can apply to epitaxial strained monolayer TMCs due to the unchanged crystal symmetry.

In the previous experimental measurement, the piezoelectric stress coefficient e_{11} in monolayer MoS_2 was measured to be 290 pC/m.[29] Other DFT calculations showed that e_{11} of pristine MoS_2 is in the range of 316 – 364 pC/m.[15,30,31] Our calculations predict that the e_{11} of pristine MoS_2 is 322 pC/m, which agrees with previous experimental and computational results. Most of the piezoelectric monolayer TMCs achieve 3-10 pV/m for d_{11} in the pristine state. Compared to other 2D piezoelectric materials, the d_{11} of group II chalcogenides, such as MgSe, CaS, and ZnS, are reported in the range of 5-25 pm/V.[32] The d_{11} of group II oxides and group III-V are reported in the range of 0.02-5.50 pm/V.[15]

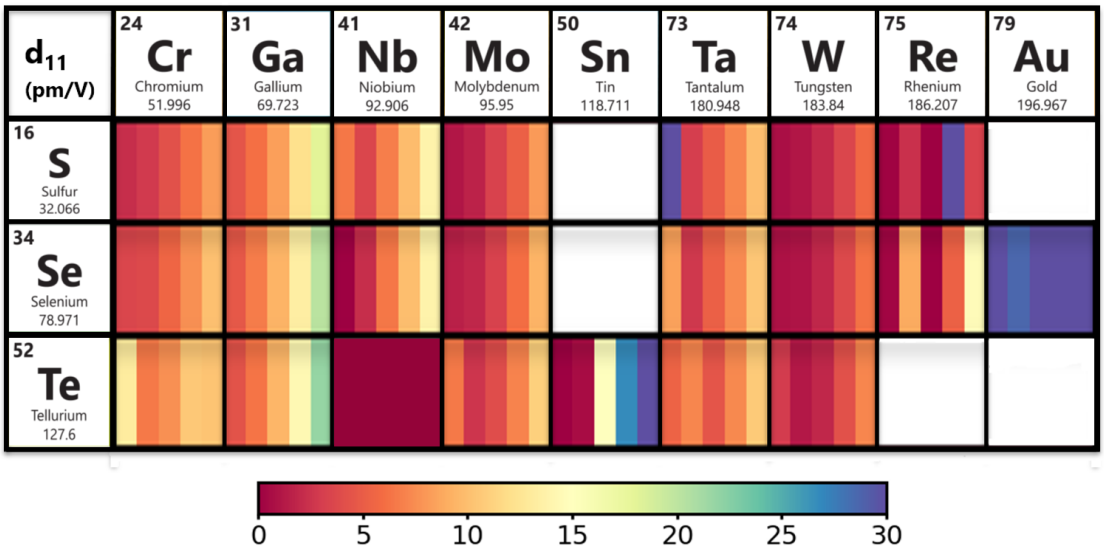

Figure 6. Piezoelectric coefficient of calculated non-centrosymmetric monolayer TMCs, d_{11}, in units of pm/V. The color changes within each box corresponding to the -10%, -5%, 0%, 5%, 10% epitaxial strained state from left to right, respectively. The blank boxes represent no stable 2D monolayer structures exists in the composition.

In Figure 6, only 22 of the 56 calculated monolayer TMCs potentially possess piezoelectric property, and the piezoelectric coefficient d_{11} is obtained at different epitaxial strained states. The epitaxial strain generally has a positive nonlinear relationship with the piezoelectric coefficient. Interestingly, except Sn, Re, Au-based monolayer TMCs, the d_{11} can increase by over 100% and even 200% at 10% epitaxial strain. This dramatic change of piezoelectric coefficient mainly comes from both elastic and piezoelectric tensor at strained state. The elastic constant C_{11} is inversely related to E_x, where E_x is the Young's modulus in in-plane direction. As the epitaxial strain increases, the E_x increases due to the higher interatomic potential in the in-plane direction; therefore, the C_{11} decreases in almost all the TMCs. The change of elastic constant C_{12} from the strain is found to be much smaller than C_{11} in most cases. The piezoelectric stress coefficient e_{11} mostly increases as epitaxial strain increases. Overall, based on the relationship between epitaxial strain and components to derive d_{11}, the d_{11} is predicted to increase as epitaxial strain increases.

This specific trend can apply to most of TMCs because the crystal structures in 2D form share very similar point group.

Similar to the interatomic potential, the piezoelectric coefficient of Re-based TMCs has a relatively complicated response to epitaxial strain because the elastic tensor does not follow a similar trend as other TMCs with $\bar{6}m2$ symmetry. At pristine and +5% epitaxial strain state, the d_{11} can vary from -120 pm/V to 119 pm/V so that d_{11} has an extreme point between these two states. As for the TMCs with m point group symmetry, Sn, Au-based monolayer TMCs are predicted to achieve a relatively high piezoelectric coefficient. Due to the phase transformation, the d_{11} of Sn_2Te_2 can potentially reach 15-30 pm/V from 0 to +10% epitaxial strain. At the compressive epitaxial strain, the other phases are not non-centrosymmetric. For Au_2Se_2, the d_{11} is predicted to be 326 pm/V at 5% epitaxial strain, the highest d_{11} value from all the calculated structures. Overall, the piezoelectricity is predicted to be enhanced by epitaxial strain and achieve ultra-high d_{11} coefficients for Au, Re-based monolayer TMCs.

According to the piezoelectric calculations of monolayer TMCs under -10% to 10% epitaxial strain, the d_{11} coefficients provide a much broader range, from -120 pm/V to 326 pm/V, than previous reports.[16] More importantly, the crystal structures remain the same and relatively stable. Experimentally, the ultra-large strain of WS_2 has been achieved by transferring a monolayer single crystal to polydimethylsiloxane (PDMS) substrate and elongating the substrate from a loading frame.[33] Similar experiments can possibly be applied to epitaxial strain tests. The enhanced piezoelectricity from epitaxial strain can potentially be utilized in the existing piezoelectric applications, including strain sensing[34] and energy harvesting,[35] and promising applications, including piezo-phototronics and catalysis.

Conclusions

We report stability and piezoelectric coefficients for the current library of 56 monolayer TMCs under epitaxial strain. The crystal structures and formation energy of the library are summarized and potentially used for the reference of heterostructure fabrication and epitaxial synthesis. Almost all the candidates at ±5% epitaxial strain and the majority of the candidates at ±10% epitaxial strain remain relatively stable where energy difference below 200 meV. Re-based TMCs exhibit a unique stability-strain relationship and likely develop a new metastable state under epitaxial strain. Of the 56 monolayer TMCs, 22 candidates are identified as possible 2D piezoelectric materials. Under both compressive and tensile strain, d_{11} coefficients of the candidates noticeably vary from pristine state. Especially, most of d_{11} coefficients are predicted to increase by 100-200% under tensile epitaxial strain. $ReSe_2$ at pristine state and Au_2Se_2 at +5% epitaxial strain are predicted to obtain the extreme d_{11} coefficients at -120 pm/V and 326 pm/V, respectively. This epitaxial strain engineering on monolayer TMCs probably opens a hidden door to high-performance 2D piezoelectric devices.

Methods

The density functional theory (DFT) calculations are performed under the plane-wave basis[36] and projector augmented wave (PAW)[37] method within the Vienna Ab initio Simulation Package (VASP).[38] Perdew–Burke–Ernzerhoff (PBE) generalized gradient functional[39] is chosen for exchange-correlation functional. To acquire dispersion interactions between 2D multilayers, the nonlocal vdW-DF-optB88 exchange-correlation functional is employed.[40,41] Based on the convergence tests, energies are converged to within 1 meV $atom^{-1}$ with a 600 eV cutoff energy and with a 15 × 15 × 1 k-point mesh. 20 Å of vacuum in the direction perpendicular to the interface is found to be sufficient for monolayer interaction below 1 meV $atom^{-1}$ in the periodic boundary condition. In order to explore the possibility of anisotropic elastic deformation under epitaxial strain, the supercell is expanded to 4 × 4 × 1 from the primitive unit cell. For the elastic and

piezoelectric tensor calculations, density functional perturbation theory (DFPT)[42] is applied including finite differences method. The k-point mesh and cut-off energy are increased to 25 × 25 × 1and 680 eV, respectively. The vacuum is found to be sufficient to obtain converged results. The internal strain relaxation is essential to obtain the realistic piezoelectric properties and compare with experimental values. Therefore, the relaxed-ion method is used to derive the d_{11} values. The convergence tests indicate the same k-point mesh, energy cutoff, and thickness of vacuum are sufficient to converge piezoelectric coefficient to within 1% accuracy.

Author Contributions

Y. L. conducted all calculations and analysis and S.B.S. supervised the work. All authors have given approval to the final version of the manuscript.

Acknowledgements

This work was supported by the Basic Office of Science of the Department of Energy under award DE-SC0018025. The computational work was conducted as part of The Pennsylvania State University (PSU) 2D Crystal Consortium – Materials Innovation Platform (2DCC-MIP) under NSF award No. DMR-1539916. Support was also received from the Penn State Institute for CyberScience (ICS) through a Graduate Research Assistantship. The calculations carried out for this paper were performed on the Pennsylvania State University Institute for CyberScience Advanced CyberInfrastructure (ICS-ACI). This content is solely the responsibility of the authors and does not necessarily represent the views of the ICS.

References

(1) Splendiani, A.; Sun, L.; Zhang, Y.; Li, T.; Kim, J.; Chim, C. Y.; Galli, G.; Wang, F. Emerging Photoluminescence in Monolayer MoS_2. *Nano Lett.* **2010**, *10* (4), 1271–1275.

(2) Mak, K. F.; Lee, C.; Hone, J.; Shan, J.; Heinz, T. F. Atomically Thin MoS_2: A New Direct-

Gap Semiconductor. *Phys. Rev. Lett.* **2010**, *105* (13), 136805.

(3) Manzeli, S.; Ovchinnikov, D.; Pasquier, D.; Yazyev, O. V.; Kis, A. 2D Transition Metal Dichalcogenides. *Nat. Rev. Mater.* **2017**, *2*, 17033.

(4) Lee, C.; Wei, X.; Kysar, J. W.; Hone, J. Measurement of the Elastic Properties and Intrinsic Strength of Monolayer Graphene. *Science.* **2008**, *321* (5887), 385–388.

(5) Phys, J. A. Strain Engineering in Functional 2- Dimensional Materials Strain Engineering in Functional 2-Dimensional Materials. **2019**, *082402* (November 2018).

(6) Gao, L. Flexible Device Applications of 2D Semiconductors. *Small* **2017**, *13* (35), 1–15.

(7) Akinwande, D.; Petrone, N.; Hone, J. Two-Dimensional Flexible Nanoelectronics. *Nat. Commun.* **2014**, *5*, 5678.

(8) Stoppa, M.; Chiolerio, A. Wearable Electronics and Smart Textiles: A Critical Review. *Sensors (Switzerland)* **2014**, *14* (7), 11957–11992.

(9) Windmiller, J. R.; Wang, J. Wearable Electrochemical Sensors and Biosensors: A Review. *Electroanalysis* **2013**, *25* (1), 29–46.

(10) Hammock, M. L.; Chortos, A.; Tee, B. C. K.; Tok, J. B. H.; Bao, Z. 25th Anniversary Article: The Evolution of Electronic Skin (E-Skin): A Brief History, Design Considerations, and Recent Progress. *Adv. Mater.* **2013**, *25* (42), 5997–6038.

(11) Conley, H. J.; Wang, B.; Ziegler, J. I.; Haglund, R. F.; Pantelides, S. T.; Bolotin, K. I. Bandgap Engineering of Strained Monolayer and Bilayer MoS_2. *Nano Lett.* **2013**, *13* (8), 3626–3630.

(12) Johari, P.; Shenoy, V. B. Tuning the Electronic Properties of Semi- Conducting Transition Metal Dichalcogenides by Applying Mechanical Strains. *ACS Nano* **2012**, *6* (6), 5449–5456.

(13) Ji, Q.; Zhang, Y. Y.; Gao, T.; Zhang, Y. Y.; Ma, D.; Liu, M.; Chen, Y.; Qiao, X.; Tan, P. H.; Kan, M.; Feng, J.; Sun, Q.; Liu, Z. Epitaxial Monolayer MoS_2 on Mica with Novel Photoluminescence. *Nano Lett.* **2013**, 13 (8), 3870–3877.

(14) Aretouli, K. E.; Tsoutsou, D.; Tsipas, P.; Marquez-Velasco, J.; Aminalragia Giamini, S.; Kelaidis, N.; Psycharis, V.; Dimoulas, A. Epitaxial 2D $SnSe_2$/ 2D WSe_2 van Der Waals Heterostructures. *ACS Appl. Mater. Interfaces* **2016**, *8* (35), 23222–23229.

(15) Blonsky, M. N.; Zhuang, H. L.; Singh, A. K.; Hennig, R. G. Ab Initio Prediction of Piezoelectricity in Two-Dimensional Materials. *ACS Nano* **2015**, *9* (10), 9885–9891.

(16) Hinchet, R.; Khan, U.; Falconi, C.; Kim, S. W. Piezoelectric Properties in Two-Dimensional Materials: Simulations and Experiments. *Mater. Today* **2018**, *21* (6), 611–630.

(17) Pospischil, A.; Furchi, M. M.; Mueller, T. Solar-Energy Conversion and Light Emission in an Atomic Monolayer p-n Diode. *Nat. Nanotechnol.* **2014**, *9* (4), 257–261.

(18) Wu, W.; Wang, Z. L. Piezotronics and Piezo-Phototronics for Adaptive Electronics and Optoelectronics. *Nat. Rev. Mater.* **2016**, *1* (7), 16031.

(19) Ong, M. T.; Reed, E. J. Engineered Piezoelectricity in Graphene. *ACS Nano* **2012**, *6* (2), 1387–1394.

(20) Zhang, F.; Lu, Y.; Schulman, D. S.; Zhang, T.; Fujisawa, K.; Lin, Z.; Lei, Y.; Elias, A. L.;

Das, S.; Sinnott, S. B.; Terrones, M. Carbon Doping of WS_2 Monolayers: Bandgap Reduction and p-Type Doping Transport. *Sci. Adv.* **2019**, *5* (5).

(21) Wang, S.; Robertson, A.; Warner, J. H. Atomic Structure of Defects and Dopants in 2D Layered Transition Metal Dichalcogenides. *Chem. Soc. Rev.* **2018**, *47* (17), 6764–6794.

(22) Zhou, J.; Wang, H.; Liu, F.; Fu, Q.; Zeng, Q.; Liu, Z.; Lin, J.; Suenaga, K.; Huang, X.; Yang, C.; Lu, L.; Yu, T.; Shen, Z.; Lin, H; Yakobson, B.; Liu, Q.; Suenaga, K; Liu, G.; Liu, Z. A Library of Atomically Thin Metal Chalcogenides. *Nature* **2018**, *556* (7701), 355–359.

(23) Mounet, N.; Gibertini, M.; Schwaller, P.; Campi, D.; Merkys, A.; Marrazzo, A.; Sohier, T.; Castelli, I. E.; Cepellotti, A.; Pizzi, G.; Marzari, N. Two-Dimensional Materials from High-Throughput Computational Exfoliation of Experimentally Known Compounds. *Nat. Nanotechnol.* **2018**, *13* (3), 246–252.

(24) Hellenbrandt, M. The Inorganic Crystal Structure Database (ICSD) - Present and Future. *Crystallogr. Rev.* **2004**, *10* (1), 17–22.

(25) Ding, H.; Dwaraknath, S. S.; Garten, L.; Ndione, P.; Ginley, D.; Persson, K. A. Computational Approach for Epitaxial Polymorph Stabilization through Substrate Selection. *ACS Appl. Mater. Interfaces* **2016**, *8* (20), 13086–13093.

(26) Parr, R. G. Density Functional Theory of Atoms and Molecules. In *Horizons of Quantum Chemistry: Proceedings of the Third International Congress of Quantum Chemistry Held at Kyoto, Japan, October 29 - November 3, 1979*; Fukui, K., Pullman, B., Eds.; Springer Netherlands: Dordrecht, 1980; pp 5–15.

(27) Zhang, Q.; Chang, Z.; Xu, G.; Wang, Z.; Zhang, Y.; Xu, Z. Q.; Chen, S.; Bao, Q.; Liu, J. Z.; Mai, Y. W.; Duan, W.; Fuhrer, M, S.; Zheng, C. Strain Relaxation of Monolayer WS_2 on Plastic Substrate. *Adv. Funct. Mater.* **2016**, *26* (47), 8707–8714.

(28) Blonsky, M. N.; Zhuang, H. L.; Singh, A. K.; Hennig, R. G. Ab Initio Prediction of Piezoelectricity in Two-Dimensional Materials. *ACS Nano* **2015**, *9* (10), 9885–9891.

(29) Zhu, H.; Wang, Y.; Xiao, J.; Liu, M.; Xiong, S.; Wong, Z. J.; Ye, Z.; Ye, Y.; Yin, X.; Zhang, X. Observation of Piezoelectricity in Free-Standing Monolayer MoS_2. *Nat. Nanotechnol.* **2015**, *10* (2), 151–155.

(30) Alyörük, M. M.; Aierken, Y.; Çaklr, D.; Peeters, F. M.; Sevik, C. Promising Piezoelectric Performance of Single Layer Transition-Metal Dichalcogenides and Dioxides. *J. Phys. Chem. C* **2015**, *119* (40), 23231–23237.

(31) Michel, K. H.; Çaklr, D.; Sevik, C.; Peeters, F. M. Piezoelectricity in Two-Dimensional Materials: Comparative Study between Lattice Dynamics and Ab Initio Calculations. *Phys. Rev. B* **2017**, *95* (12), 125415.

(32) Sevik, C.; Çaklr, D.; Gülseren, O.; Peeters, F. M. Peculiar Piezoelectric Properties of Soft Two-Dimensional Materials. *J. Phys. Chem. C* **2016**, *120* (26), 13948–13953.

(33) Guo, H.; Lan, C.; Zhou, Z.; Sun, P.; Wei, D.; Li, C. Transparent, Flexible, and Stretchable WS2based Humidity Sensors for Electronic Skin. *Nanoscale* **2017**, *9* (19), 6246–6253.

(34) Wang, S.; Wang, X.; Wang, Z. L.; Yang, Y. Efficient Scavenging of Solar and Wind Energies in a Smart City. *ACS Nano* **2016**, *10* (6), 5696–5700.

(35) Wang, Z. L.; Song, J. Piezoelectric Nanogenerators Based on Zinc Oxide Nanowire Arrays.

Science. **2006**, *312* (5771), 242–246.

(36) Kresse, G.; Furthmüller, J. Efficient Iterative Schemes for Ab Initio Total-Energy Calculations Using a Plane-Wave Basis Set. *Phys. Rev. B - Condens. Matter Mater. Phys.* **1996**, *54* (16), 11169–11186.

(37) Blöchl, P. E. Projector Augmented-Wave Method. *Phys. Rev. B* **1994**, *50* (24), 17953–17979.

(38) Kresse, G.; Furthmüller, J. Software VASP, Vienna. *Phys. Rev. B* **1996**.

(39) Perdew, J. P.; Burke, K.; Ernzerhof, M. Generalized Gradient Approximation Made Simple. *Phys. Rev. Lett.* **1996**, *77* (18), 3865–3868.

(40) Dion, M.; Rydberg, H.; Schröder, E.; Langreth, D. C.; Lundqvist, B. I. Van Der Waals Density Functional for General Geometries. *Phys. Rev. Lett.* **2004**, *92* (24), 246401.

(41) Klime, J.; Bowler, D. R.; Michaelides, A. Van Der Waals Density Functionals Applied to Solids. *Phys. Rev. B - Condens. Matter Mater. Phys.* **2011**, *83* (19), 195131.

(42) Baroni, S.; De Gironcoli, S.; Dal Corso, A.; Giannozzi, P. Phonons and Related Crystal Properties from Density-Functional Perturbation Theory. *Rev. Mod. Phys.* **2001**, *73* (2), 515–562.